Ice crystals accretion capabilities of ONERA's 3D icing suite

Claire Laurent, Maxime Bouyges, Virgile Charton, Lokman Bennani, Jean-Mathieu Senoner

Ice crystals accretion capabilities of ONERA's 3D icing suite

Claire Laurent*, Maxime Bouyges†, Lokman Bennani‡ and Jean-Mathieu Senoner§
ONERA – The French Aerospace Lab, F-31055, Toulouse, France

Virgile Charton¶
ONERA, Université Paris Saclay, F-91123, Palaiseau, France

In the framework of the MUSIC-haic European project, the ONERA 3D accretion solver FILM has been enhanced with ICI (Ice Crystal Icing) capabilities. These new features target different phenomena such as ice layer porosity, erosion due to ice crystals impacts, and also heat transfers with the solid surface. In ICI simulations, the erosion phenomena plays an active role on the ice shape, creating conical shapes which have been extensively studied. However, these shapes are currently modeled using a multi-step approach which requires a re-meshing procedure at each time step. Such a procedure, involving recomputing the flow-field and particle trajectories, would be very expensive for 3D simulations. The first part of this article is then devoted to present a new geometrical approach which is promising to take into account the erosion effect on the ice shape for 3D simulations without re-meshing. The other key point for ICI simulations is the modeling of thermal coupling with the wall. Indeed, this phenomenon is essential for simulations in engine environment or on anti-iced airfoils. The second part of the article is then dedicated to the implementation of an efficient algorithm for the thermal coupling with a 3D heat conduction solver.

I. Nomenclature

IAC = Impact Angle Correction
ICI = Ice Crystal Icing
MS = Multi-Step
OS = One-Step

II. Introduction

In the framework of MUSIC-haic European project, the 3D ONERA accretion tools have been updated with ICI models developed during the HAIC and MUSIC-haic projects. ICI models have been implemented in the FILM solver which is the ONERA accretion tool mainly used for simulations of accretion in turbojet engines. New specific methodologies presented in this paper have been developed to allow efficient 3D simulations.

The first one consists in a geometrical algorithm implemented in the Messinger energy balance in order to reproduce the erosion effect on the ice shape. This erosion effect creates the well-known conical ice shapes. This new geometrical method is called Impact Angle Correction (IAC) method. It allows to take into account the evolution of the ice shape in the erosion modeling. Thus, it is possible to obtain conical ice shapes without using a multi-step (MS) approach which requires a re-meshing procedure at each time step. This method has been first evaluated for 2D calculations and then extended on 3D simulations. The results of this method applied to the hemispherical test-case studied by Currie *et al.* [1] are presented in the first part of the article.

The second part concerns the thermal coupling at the wall. This coupling is determining in engines environment to simulate the thermal exchanges between the liquid/ice layer and the solid wall. A specific procedure has been implemented to couple the FILM solver with a heat conduction solver. Validation test-cases have been performed and results including comparisons with experimental data are presented.

*Research Engineer, PhD, Multi-physics Dept., 2 avenue Edouard Belin, Toulouse, France
†Research Engineer, PhD, Multi-physics Dept., 2 avenue Edouard Belin, Toulouse, France
‡Research Engineer, PhD, Multi-physics Dept., 2 avenue Edouard Belin, Toulouse, France
§Research Engineer, PhD, Multi-physics Dept., 2 avenue Edouard Belin, Toulouse, France
¶Research Engineer, PhD, Multi-physics Dept., 6 chemin de la Vauve aux Granges, Palaiseau, France

III. Presentation of the Film accretion solver

A. Background

The Film solver is a 3D surface solver of ONERA's multi-physics Cedre platform [2]. This solver uses an integral eulerian approach to solve wall liquid films and accretion equations over a 3D wall surface. The solver was first developed to simulate water ingestion in turbojet engines (thus containing all functionalities necessary for rotating frames) and has been then upgraded to include a two-layer accretion model for icing simulations [3]. The Film geometry (a surface mesh) is built from the Cedre geometry (a general unstructured volume mesh) and it is partitioned for parallel computations. Concerning modeling aspects, the Film solver is coupled with the gas phase solver Charme to compute the shear driven force, the gas pressure gradient acting on the film motion as well as the heat and the mass transfers coefficients for the calculation of exchanges with the air flow. The source terms for the disperse phase are obtained using either Spiree, Cedre's eulerian dispersed solver, or Sparte, Cedre's lagrangian solver. In the framework of the HAIC European project, models for trajectory and melting of ice crystals [4–6] were implemented in the Sparte solver [7]. In the Film solver, the modeling of accretion is performed by distinguishing between four accretion regimes: full-evaporative regime (dry wall), running wet conditions (only a wall liquid film), rime ice conditions (only ice with a negative temperature) and glaze ice conditions (porous ice at the wall with a liquid film above, both at the melting temperature T_f.) [3]. The source terms for ice crystals have been added to the equations for each regime. The deposition rates are either computed by Sparte (in glaciated conditions which do not require a coupled algorithm) or by Film from the impingement fluxes provided by Sparte (both for glaciated and mixed phase conditions). The following subsections describe the implemented models with more detail.

B. Film accretion model

In the Film solver, the accretion is modeled by two layers, a porous ice layer at the wall and a liquid layer. The liquid layer is modeled by a running liquid film using the shallow water equations. Depending on the regime, there is only an ice layer (rime ice), only a liquid film layer (running wet), no layer (full evaporation) or both layers (glaze ice). In this article, a focus is done on the glaze ice regime which is the most common for ice crystals accretion. In this model, the thermal gradient inside the ice layer is neglected* and the erosion and porosity phenomena have to be taken into account. Then, the unknowns of the system are the solid thickness h_s, the liquid thickness h_l which is divided into the running liquid film thickness $h_{l,r}$ and the equivalent liquid thickness for the accumulated water in the porous ice layer $h_{l,acc}$, ie $h_l = h_{l,r} + h_{l,acc}$. The global mass equation for this regime is written below

$$\frac{\partial}{\partial t}\left(\rho_l h_l + \rho_s h_s\right) + div_t\left(\rho_l h_{l,r}\vec{\boldsymbol{v}}_{\boldsymbol{t,l}}\right) = \Phi_{dep,m,l} + \Phi_{dep,m,s} - \Phi_{ev} - \Phi_{er}. \tag{1}$$

This equation is equivalent to

$$\frac{\partial}{\partial t}\left(\rho_l h_l + \rho_s h_s\right) = \Phi_{tot,m} - \Phi_{rout,m,l} - \Phi_{er} \tag{2}$$

with the following definition for the total mass flow rate

$$\Phi_{tot,m} = \Phi_{rin,m,l} + \Phi_{dep,m,l} + \Phi_{dep,m,s} - \Phi_{ev} \tag{3}$$

where $\vec{\boldsymbol{v}}_{\boldsymbol{t,l}}$ is the tangential† velocity of the liquid, $\Phi_{rin,m,l}$ is the mass source term for the incoming running liquid film, $\Phi_{rout,m,l}$ for the outgoing running liquid film, Φ_{dep} for the ice crystals deposition, Φ_{ev} for the evaporation and Φ_{er} for the erosion. The mass fluxes terms $\Phi_{rin,m,l}$ and $\Phi_{rout,m,l}$ are obtained from the momentum equation written for the running liquid film (see [3]), Φ_{ev} is modeled using the Chilton-Colburn analogy (see [3]) and the deposition flux Φ_{dep} using the HAIC sticking efficiency model $\Phi_{dep} = \epsilon_S \Phi_{imp}$:

$$\epsilon_S = (K_C - 2)\eta_m^3 + (3 - 2K_C)\eta_m^2 + K_C\eta_m \tag{4}$$

with $K_C = 2.5$ [6]. The erosion model is described in the next subsection.

Then, the global enthalpy equation for both liquid and solid layers is

$$\begin{aligned}\frac{\partial}{\partial t}\left(\rho_l h_l \eta_l + \rho_s h_s \eta_s\right) + div_t\left(\rho_l h_{l,r}\eta_l \vec{\boldsymbol{v}}_{\boldsymbol{t,l}}\right) = \Phi_{dep,\eta,l} + \Phi_{dep,\eta,s} - \Phi_{ev}\eta_v + \\ H_{t,g}(T_{r,g} - T_m) + H_{t,w}(T_{r,w} - T_m) - \Phi_{er,l}\eta_l - \Phi_{er,s}\eta_s\end{aligned} \tag{5}$$

*The temperature is assumed uniform and constant equal to the melting temperature T_m.

†Recall that these are surface equations.

which is equivalent to

$$\frac{\partial}{\partial t}\left(\rho_l h_l \eta_l + \rho_s h_s \eta_s\right) = \Phi_{tot,\eta} - \Phi_{rout,m,l}\eta_l - \Phi_{er,l}\eta_l - \Phi_{er,s}\eta_s \tag{6}$$

with the following definition for the total enthalpy flow rate

$$\Phi_{tot,\eta} = \Phi_{rin,\eta,l} + \Phi_{dep,\eta,l} + \Phi_{dep,\eta,s} - \Phi_{ev}\eta_v + H_{t,g}(T_{r,g} - T_m) + H_{t,w}(T_{r,w} - T_m) \tag{7}$$

The heat exchanges with the gas and the wall are respectively modeled by a heat exchange coefficient $H_{t,g}$ for the gas and $H_{t,w}$ for the wall and a recovery temperature $T_{r,g}$ for the gas and $T_{r,w}$ for the wall. The enthalpy of the solid, the liquid and the vapor phases are defined by

$$\eta_s(T) = Cp_s(T - T_m) \tag{8}$$

$$\eta_l(T) = Cp_l(T - T_m) + L_f(T_m) \tag{9}$$

$$\eta_v(T) = Cp_v(T - T_b) + L_v(T_b) + Cp_l(T_b - T_m) + L_f(T_m) \tag{10}$$

with T_m the melting temperature and T_b the boiling point. With this choice for the reference of enthalpy functions, it appears that for glaze ice regime, $\eta_s(T_m) = 0$ and $\eta_l(T_m) = L_f(T_m) = L_f$. Then, the global enthalpy equation (5) can be simplified into

$$L_f \frac{\partial}{\partial t}\left(\rho_l h_l\right) = \Phi_{tot,\eta} - \Phi_{rout,m,l}L_f - \Phi_{er,l}L_f \tag{11}$$

Finally, it leads to the mass conservation equation for the liquid phase, both for the film running water and the accumulated water :

$$\frac{\partial \rho_l h_l}{\partial t} = \Phi_{tot,m,l} - \Phi_{rout,m,l} - \Phi_{er,l} \tag{12}$$

with the following definition for the total liquid mass flow rate

$$\Phi_{tot,m,l} = \frac{\Phi_{tot,\eta}}{L_f} \tag{13}$$

Then, to split the liquid water between the running film and the water accumulated in the porous ice layer, the coupled erosion-porosity model has to be applied (see next subsection). The height of accumulated water depends on the height of the solid ice layer h_s .

The mass conservation equation for the solid phase is derived by subtracting equation (12) obtained for the liquid mass evolution from the enthalpy global balance (1), and it gives

$$\frac{\partial \rho_s h_s}{\partial t} = \Phi_{tot,m,s} - \Phi_{er,s} \tag{14}$$

with

$$\Phi_{tot,m,s} = \Phi_{tot,m} - \Phi_{tot,m,l} = \frac{\Phi_{tot,m}L_f - \Phi_{tot,\eta}}{L_f} \tag{15}$$

Then, the erosion model will enable to calculate the solid ice thickness h_s. This model is coupled with the porosity model since ice material properties used in the erosion model are depending of the porosity liquid fraction.

C. Erosion and porosity models

Regarding the erosion phenomenon, both liquid and solid water are removed. The distribution between the two phases is computed according to the liquid fraction f_l defined by the ratio between the liquid mass flux and the total mass flux, such as

$$f_l = \frac{\Phi_{tot,m,l}}{\Phi_{tot,m}} \tag{16}$$

assuming that the ice growth is a steady phenomenon. Thus, this liquid fraction f_l is used to spread the erosion mass loss between liquid and solid as follows

$$\Phi_{er,s} = (1 - f_l)\Phi_{er} \tag{17}$$

$$\Phi_{er,l} = f_l\Phi_{er} \tag{18}$$

Moreover, the total mass erosion flux Φ_{er} depends on the porosity liquid fraction α_l defined by the ratio between the liquid accumulated water $h_{l,acc}$ and the total accumulated water in the ice layer, both liquid and solid

$$\alpha_l = \frac{\rho_l h_{l,acc}}{\rho_l h_{l,acc} + \rho_s h_s} \tag{19}$$

These quantities are evaluated after taking into account the erosion losses, using equations (12) and (14) and then applying the porosity model to separate the running liquid water from the accumulated water. Consequently, the erosion and the porosity models are coupled.

For the erosion modeling, the semi-empirical model of Charton *et al.* [8], based on the theoretical considerations on solid-solid impact proposed by Finnie and Bitter [9–11], has been implemented in Film. In this model, two main mechanisms characterize impact driven erosion phenomenon : deformation and cutting. Erosion occurs when the particle normal velocity V_n is greater than the ice elastic limit velocity V_{el}. The volumes eroded by cutting Vol_C and deformation Vol_D enable to compute the erosion flux

$$\Phi_{er} = F_s\rho_s(Vol_C + Vol_D) \tag{20}$$

where F_s is a sharpness factor depending of the sphericity factor. Detailed expression of Vol_C and Vol_D are given in [8]. The model was further developped in [12] to take into account the effect of particle diameter on erosion. To this purpose, the energy dissipated by the particle fragmentation is modeled through an "effective" particle velocity. This velocity corresponds to the velocity of the particle when the energy dissipated by its fragmentation is subtracted from its kinetic energy. As the energy dissipated depends of the damaged volume, the resulting erosion model depends on the particle diameter. Then, the effect of ice porosity is also modeled through correction coefficients on the Young modulus and the elastic limit of ice with respective to liquid mass fraction α_l.

The porosity model implemented in the Film solver is described in [6]. The maximum amount of accumulated water is a function of the ice porosity Ψ and the liquid deposition fraction ξ_l:

$$h_{l,acc,max} = h_s\frac{\Psi}{1 - \Psi}(1 - \xi_l^2) \tag{21}$$

In the model, $\Psi = 0.5$ and ξ_l is defined by

$$\xi_l = \frac{\Phi_{dep,m,l}}{\Phi_{dep,m,l} + \Phi_{dep,m,s}} \tag{22}$$

The solid height h_s is evaluated after subtracting the solid erosion loss from the equation (14). The same goes for the liquid height h_l : it is evaluated after having subtracted the liquid erosion loss from the equation (12). In the case where $h_l < h_{l,acc,max}$, $h_{l,acc}$ is set to h_l and $h_{l,r} = \Phi_{rout,m,l} = 0$. Otherwise if $h_l > h_{l,acc,max}$, therefore $h_{l,acc} = h_{l,acc,max}$ and the running liquid film has to be solved by the shallow water equations (see [3]). The iterative procedure for the coupling of erosion and porosity models is summarized on figure 1.

IV. Impact Angle Correction method

A. Issue

On classic icing codes, the Multi-Step (MS) method is used to model the effect of ice growth on the aerodynamic field and on the crystals trajectories. This method consists in dividing the accretion time into N time steps and performing a complete calculation cycle at each iteration (mesh, aerodynamics, trajectory and accretion). However, this method is quite complex and costly to extend to 3D simulations, since it requires to re-mesh at each time step. But the coupling effects involved by the ice growth are of major importance, as illustrated on figure 2. On this figure, the ice shape of test RUN67 obtained with a One-Step (OS) method (which corresponds to a single calculation with a time step equal to

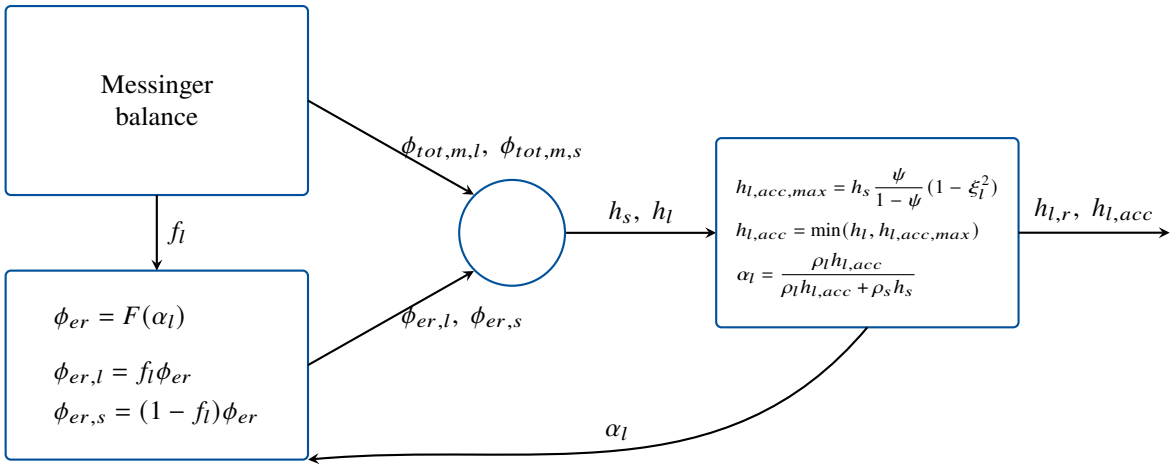

Fig. 1 Iterative procedure for the coupling between erosion and porosity models.

the accretion time) is compared to the ice shape using the MS approach. It shows that the OS method overestimates the mass and the thickness of the ice and cannot reproduce the pointed ice shape obtained experimentally. For ICI simulations, the erosion is one of the major phenomenon acting on the ice shape. The erosion is mainly driven by the magnitude and the direction of the particle velocity. It is important to notice that the normal and the tangential components of the particle velocities evolve with the ice shape. The concept of the Impact Angle Correction (IAC) method is then to model this effect by rebuilding the ice shape profile in order to calculate the normal and the tangential particle velocities during the accretion.

B. Description of the IAC method

Figure 3 shows the distribution between the rate of erosion controlled by the particles tangential velocity (cutting phenomenon) and by the particles normal velocity (plastic deformation phenomenon) from the Finnie-type erosion model. For this test, the geometry of the profile with a cylindrical leading edge leads to a loss of material by the cutting phenomena greater than by the plastic deformation, except in the vicinity of the stagnation point where the tangential velocity of the impacting particles decreases. Also, the conical shape of the ice seems to be obtained by the effect of erosion: the erosion rate is maximum for oblique impact angles, which promotes ice growth in the impact region with normal angles. In order to reproduce the conical characteristic of the ice shape, the proposed method consists in dividing the accretion time into N time steps. At each time step, the angle between the particle impact velocity vector and the ice shape normal vector is updated. Hence this allows to update the collection efficiency and the erosion rates. The key is that at the end of the time step, ice grows and the ice shape normal vector is recomputed. Thus, this method, called the Impact Angle Correction method, makes possible to take into account the evolution of the impact angle at each iteration, shaping the ice shape, without re-meshing the domain or recalculating the aerodynamic field or the crystals trajectories. The ice growth is thus reduced in areas where the angle of impact is such as the erosion is maximum, namely for grazing angles. On the contrary, cells near the stagnation point with almost normal impact angles have a minimum erosion rate, which leads to the formation of a conical ice shape.

The steps of the IAC method are mapped on figure 4 and detailed below:

- calculation of the ice thickness;
- calculation of the ice thickness gradients and update of the ice shape normal vectors with respect to the clean profile;
- calculation of the new normal and tangential components of crystal velocities to update collection efficiency and erosion model;
- new accretion calculation for the current time step with the collection efficiency and the erosion calculated in the previous step;
- update of the ice thickness on the clean profile.

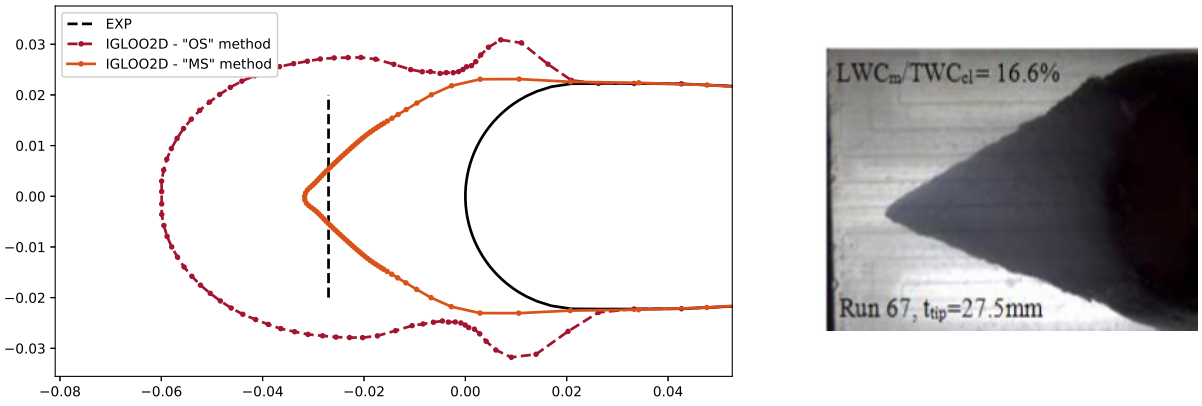

Fig. 2 Comparison between the ice shapes simulated with the 2D One-Step (OS) method and the 2D Multi-Step (MS) approach with the experimental ice thickness (maximum value given by the dotted black line) for the test RUN67 [13].

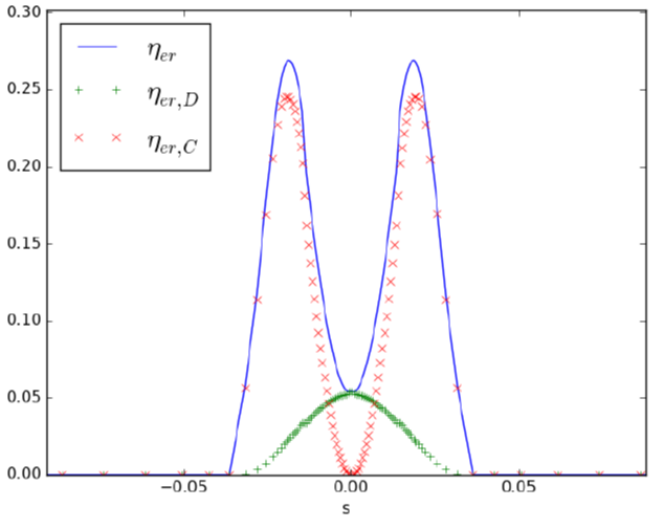

Fig. 3 Distribution of the total erosion rate between cutting and plastic deformation phenomena.

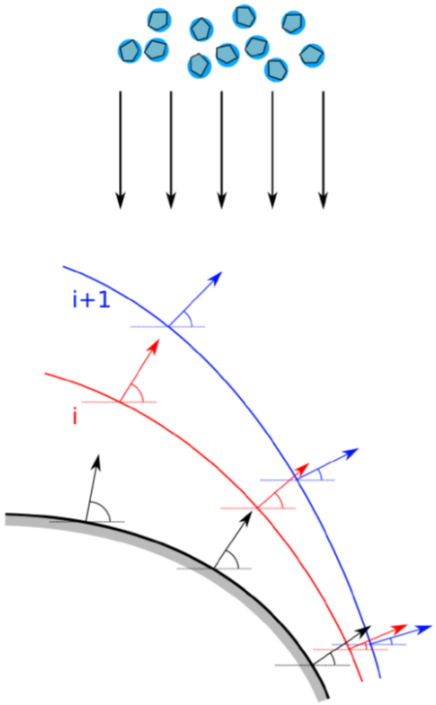

Fig. 4 Diagram of the iterative calculation of the Impact Angle Correction (IAC) method, the angle of impact is more and more shaving as iterations are performed.

C. 2D test-cases

Preliminary tests were carried out with 2D simulations for tests RUN67 and RUN1286 of Currie *et al.* experiments [1, 13–15].

Figure 5 shows the application of the IAC method for the simulation of test RUN67 [13] ($M = 0.25$, $T_i = 288.15\,\mathrm{K}$, $P_i = 34.50\,\mathrm{kPa}$, $RH = 0.28$, $TWC = 6\,\mathrm{g/m^3}$, $LWC/TWC = 0.166$, $MVD = 57\,\mu\mathrm{m}$, accretion time= 382 s) and figure 6 corresponds to the simulation of test RUN1286 [15] ($M = 0.25$, $T_i = 288.15\,\mathrm{K}$, $P_i = 34.50\,\mathrm{kPa}$, $RH = 0.18$, $TWC = 7.6\,\mathrm{g/m^3}$, $LWC/TWC = 0.07$, $MVD = 57\,\mu\mathrm{m}$, accretion time = 230 s). The results are compared with the OS and MS simulations of the IGLOO2D tool. The ice shapes obtained with the IAC method present a cone at the stagnation point and give a good approximation of the shapes obtained by the MS method of IGLOO2D. Moreover the restitution time for the IAC simulations using this geometrical method is much faster than the MS method since the re-meshing procedure[‡] is skipped.

D. 3D test-case

The hemispherical test-case [15] has been selected in order to evaluate this method for 3D applications like probes. Figure 7 shows the limitation of the OS approach to obtain the correct accreted mass. The first challenge was to obtain a smooth field for the particle impingement using a lagrangian solver. Despite a very fine mesh, some little discrepancies were still present around the stagnation point (see figure 7), with the risk of destabilizing the IAC method. A smoothing procedure has therefore been implemented in the Film solver. It has been first applied for the calculation of the impinging fluxes (see "beta" smoothing on figure 8).

Then, the IAC method has been applied to the 3D accretion calculation on the 3D hemispherical configuration and compared to the results of the MS approach obtained on 2D simulations (see figure 9). It appears that despite a very reduced calculation time, this method could be unstable. Especially for refined mesh (see 9 and 10 with non symmetrical results). In order to improve these results, the smoothing procedure has been also applied on the ice thickness and the ice thickness gradients at each time step (see "proj" smoothing on figure 9). Now, the aim is to evaluate this method for many more cases. First to check the influence of the mesh : it seems for instance that smoothing was not necessary in

[‡]Note that re-meshing implies recomputing air flow and ice crystals trajectories.

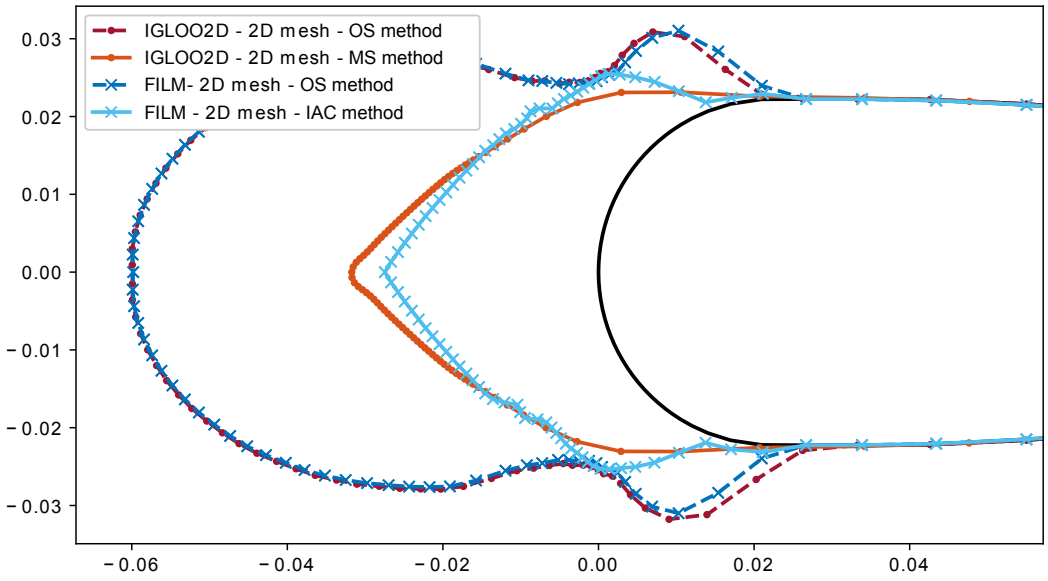

Fig. 5 Simulations of RUN67 with the One-Step (OS) and Multi-Step (MS) methods of the IGLOO2D tool with the OS and the IAC methods of the FILM solver [13].

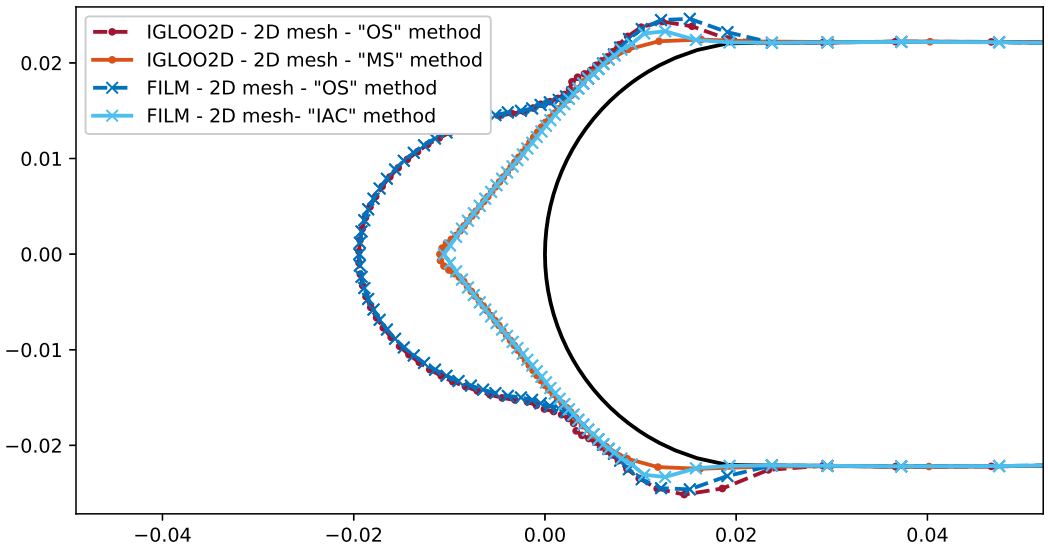

Fig. 6 Simulations of RUN1286 with the OS and MS methods of the IGLOO2D tool and with the OS and the IAC methods for the FILM solver [15].

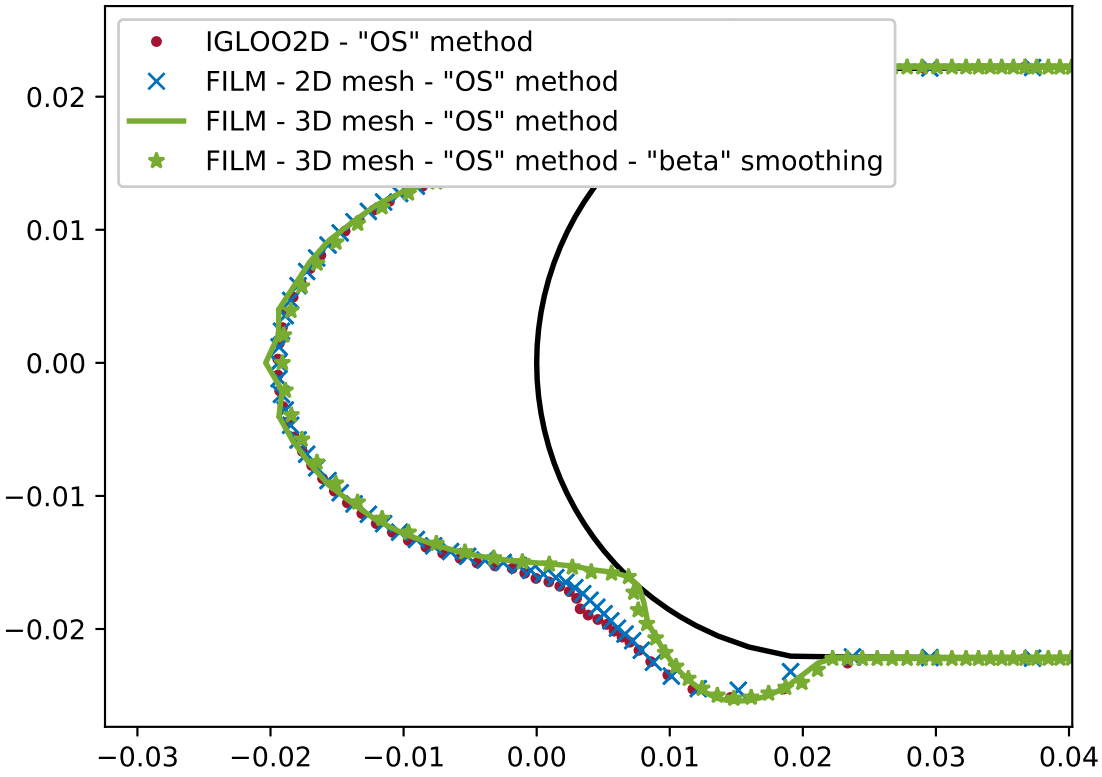

Fig. 7 One-step simulations of ice shape for the hemispherical test-case RUN1286 [15].

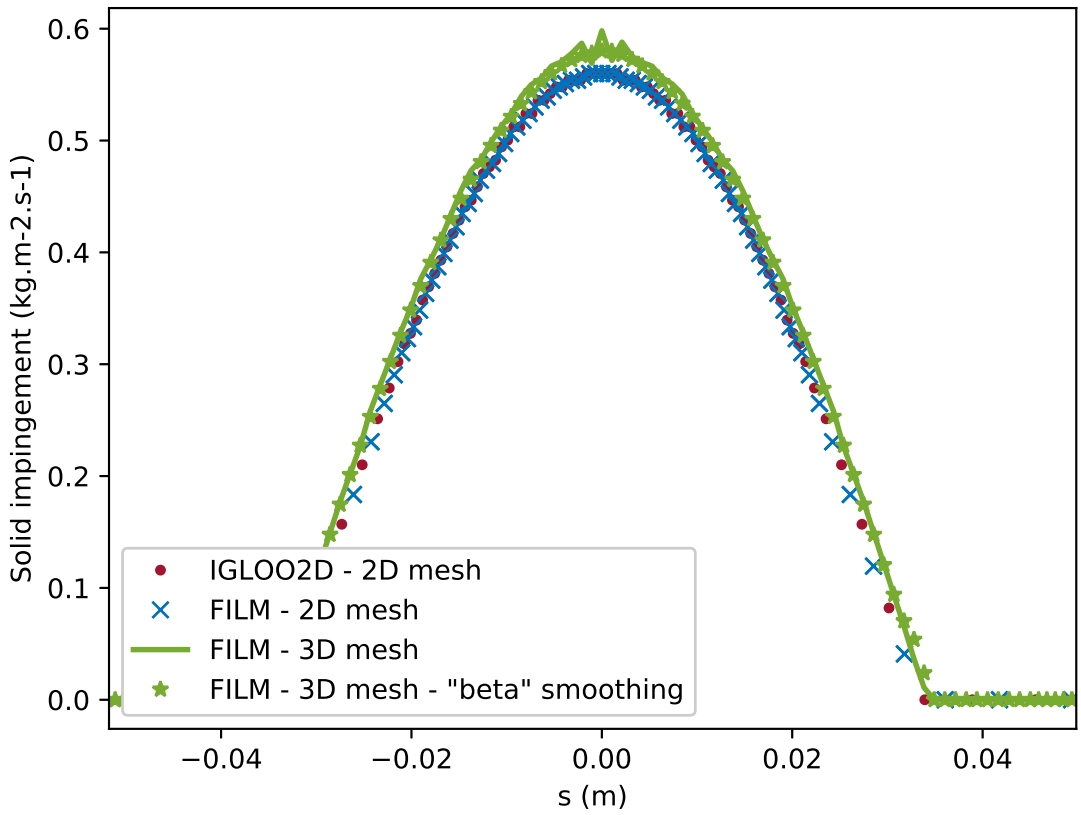

Fig. 8 Comparisons between 2D and 3D results of the solid impinging flux. Test-case RUN1286 [15].

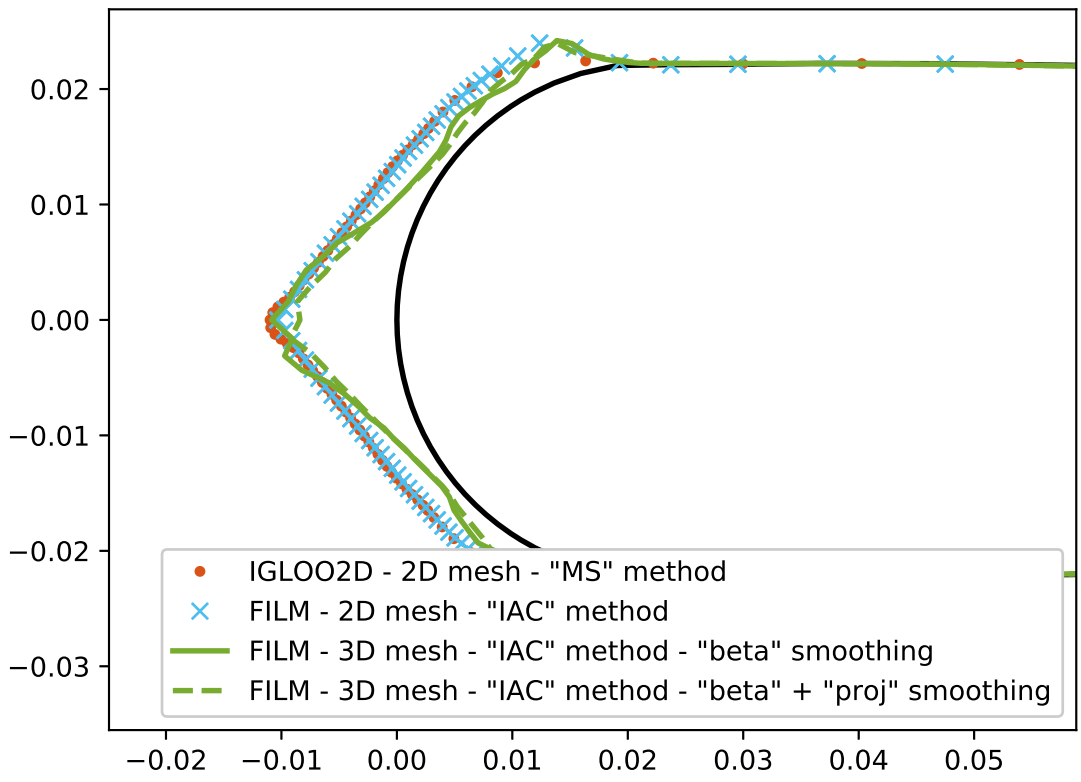

Fig. 9 Comparison between the MS approach and IAC method for the simulation of ice shape for hemispherical test-case RUN1286 [15].

2D because the mesh was coarser. And also to test the coupling of this method with other erosion models in order to analyze if this method is robust enough to be used for industrial computations and to mark out its limitations.

Finally, it should be noted that this method cannot replace an approach based on re-meshing in the case of complex geometries where the gas flow is very disturbed by ice accretion, or where the occurrence of an upstream ice shape would mask downstream accretion as it can be the case with cascading vane profiles. So despite the encouraging results obtained for tests R67 and R1286, it is important to note that this method therefore has limitations and its application for industrial purposes would require further study.

V. Coupling with a heat conduction solver

The heat transfers between the ice/liquid layer and the wall play a crucial role in the accretion phenomenon, especially if the solid material contains heating device(s) (such as bleed air, resistive heaters etc.). The heat flux received by the ice/liquid layer from the wall depends on the whole system (ice/liquid layer and solid) and necessitates the coupling between the accretion solver and the heat conduction solver in the solid.

This section details the development of the coupling between the accretion solver Film and a heat conduction solver using the ONERA coupling library CWIPI. The configuration is sketched on figure 11. A solid wall, designated as domain 1, is heated on its lower (or inner) side by a bleed air system or by thermal heaters. On the top (or exterior) side, the solid is covered by an ice layer. More precisely, this layer can either be: empty, composed of liquid water (running wet), composed of ice (rime ice) or composed of both liquid water and ice (glaze ice). This layer is referred as domain 2. Above this ice layer, an airflow carries ice crystals that may impact the layer. Different heat exchanges take place

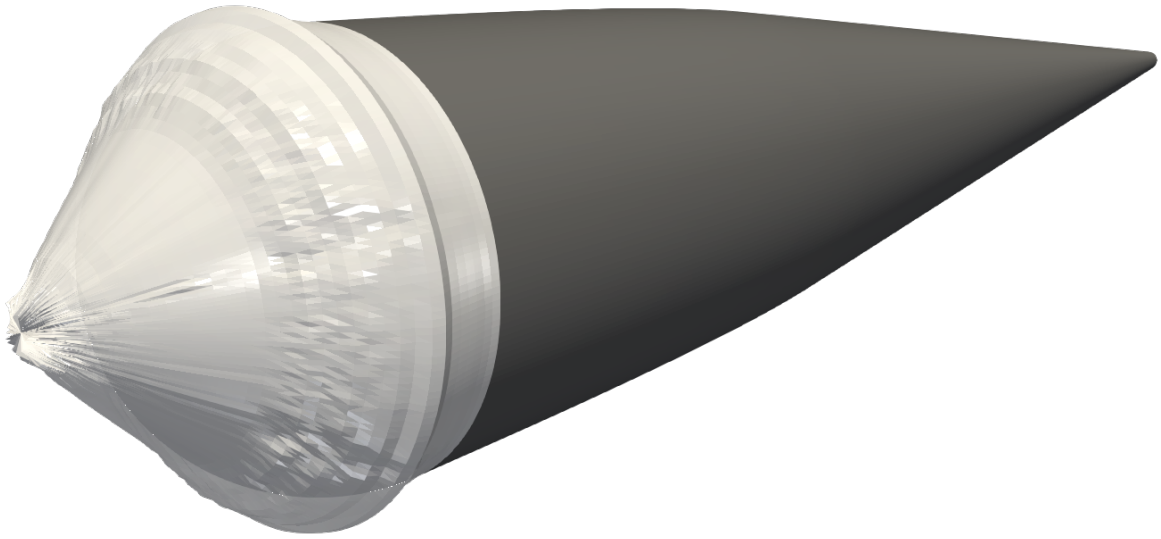

Fig. 10 3D simulation of the hemispherical test-case RUN1286 [15].

between the air flow and the ice layer: evaporation, convection, enthalpy deposition (brought by ice crystals).

The validation of the coupling methodology has been performed using ACACIA as the heat conduction solver, which is also a solver of the CEDRE platform. The coupling is generic since the use of the CWIPI library enables theoretically to couple the FILM solver with any heat conduction solver. Indeed, CWIPI is a coupling / exchange library developed at ONERA that enables two programs to exchange data in parallel. The meshes can be non-coincident and this is transparent for each solver: the CWIPI library handles the interpolation. More precisely, a default interpolation is available in the library but a user-defined interpolation scheme can also be provided. Using CWIPI as the coupling library enables each solver to "ignore" which solver it is communicating with: the different solvers only have to agree on what data they exchange and on which surface[§].

The coupling between the accretion solver and the heat conduction solver is not trivial: simply exchanging the

[§]The library can also exchange volume data.

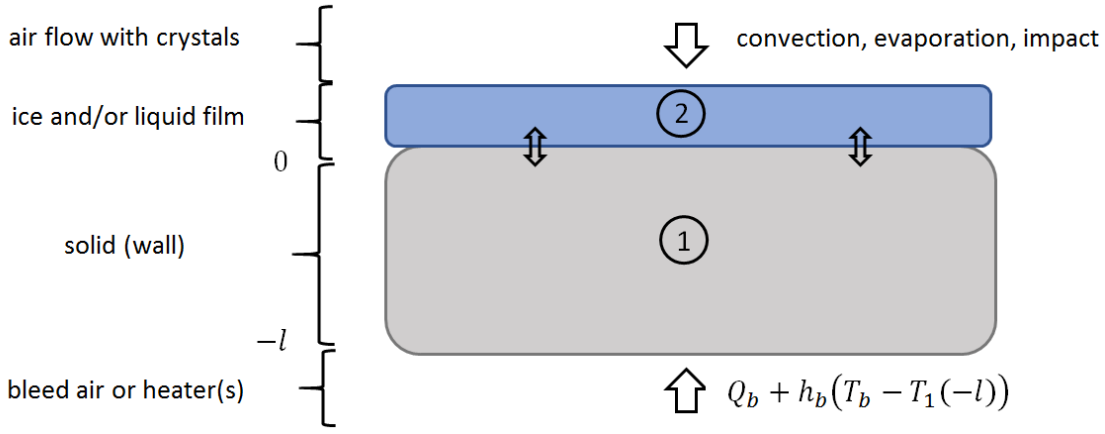

Fig. 11 Sketch of the coupling configuration between the accretion solver and the wall heat conduction solver.

temperature and the heat flux at each time step does not necessarily lead to a converged solution. Hence a specific coupling algorithm must be implemented to obtain a converged solution. Different coupling algorithms exist and have been successfully implemented in other solvers such as ONERA-IGLOO2D (see [16–18]). For a conduction problem, three different interface conditions can be used: Dirichlet, Neumann or Fourier-Robin. Coupling algorithms mostly use a Fourier-Robin interface condition:

$$\lambda \frac{\partial T}{\partial n} = Q + \omega \left(T^r - T\right), \tag{23}$$

where Q is the heat flux received from the coupled solver, ω is a coupling coefficient equivalent to a heat transfer coefficient and T^r is a "recovery temperature" or more generally the temperature of linearization. So the accretion solver sends to the heat conduction solver the three latter variables and the heat conduction solver applies the Fourier-Robin condition (and conversely). The choice of ω and the exchange chronology defines the coupling algorithm.

This paper now focuses on the Schwarz algorithm, successfully applied in ONERA-IGLOO2D and retained for the present coupling. But theoretically, Errera *et al.* strategy / coefficients could also be used as is in the present coupling. However, note that Errera *et al.* paper deals with a coupling between a heat conduction equation in a solid and an air flow, which is not identical to the present problem.

A. Schwarz coupling procedure

Consider writing the accretion solver energy balance as

$$-h_2 T_2 + \alpha_2 + Q_{1\to 2} = 0, \tag{24}$$

where h_2 represents the sum of all the linear coefficients multiplying T_2, and α_2 represents the sum of all constant terms with respect to T_2.

Then the Schwarz coupling algorithm applied to the two solvers, where k designates the coupling iteration (inside a time step), can be written as

$$\begin{cases} -h_2 T_2^{k+1}(0) + \alpha_2 + Q_{1\to 2}^{k} + \omega_2^{k}\left(T_1^{k}(0) - T_2^{k+1}(0)\right) = 0, \\ \rho_1 c_1 \dfrac{\partial T_1^{k+1}}{\partial t} = \dfrac{\partial}{\partial x}\left(\lambda_1 \dfrac{\partial T_1^{k+1}}{\partial x}\right), \\ \lambda_1 \dfrac{\partial T_1^{k+1}}{\partial x}(0) = Q_{2\to 1}^{k+1} + \omega_1^{k+1}\left(T_2^{k+1}(0) - T_1^{k+1}(0)\right), \\ -\lambda_1 \dfrac{\partial T_1^{k+1}}{\partial x}(-l) = Q_b + h_b\left(T_b - T_1^{k+1}(-l)\right). \end{cases} \tag{25}$$

Note that in the above expressions, mono-dimensional notations have been adopted to clarify the algorithm presentation. However, in both solvers the actual 3D equations are solved. This coupling algorithm is executed at each time step until a convergence criteria (on the temperature or the heat flux for instance) is reached. This means that several exchanges between the two solvers occur inside one time step. A sketch of the coupling procedure is available on figure 12.

As mentioned above, the key ingredient of the algorithm is the choice of the coefficients ω. Optimal expressions, in the sens of convergence, can be found in Bennani *et al.* paper. However, these analytic expressions can be difficult to compute, especially for 3D solvers where the definition of values such as the "local layer width" is ill-defined or hard to recover. But since the choice of ω only affects the convergence rate and not the final result, constant (user-defined) coefficients can also be applied.

B. Validation

The coupling between the accretion solver Film and the wall heat conduction solver Acacia has been validated on the test case number 2 of the work package 2 of the MUSIC-haic project. This test case has been designed, conceived and studied at TU Braunschweig by Malik *et al.* (publication is in progress). It consists in a flat plate of approximately $8\,\text{cm} \times 30\,\text{cm}$ containing a central heater 6 mm deep inside the solid. The numerical model for this configuration, as well as a side view of the mesh used for the simulation, are depicted on figure 13. The heaters, with a thickness of 0.2 mm, are located between the beige area and the dark-blue one.

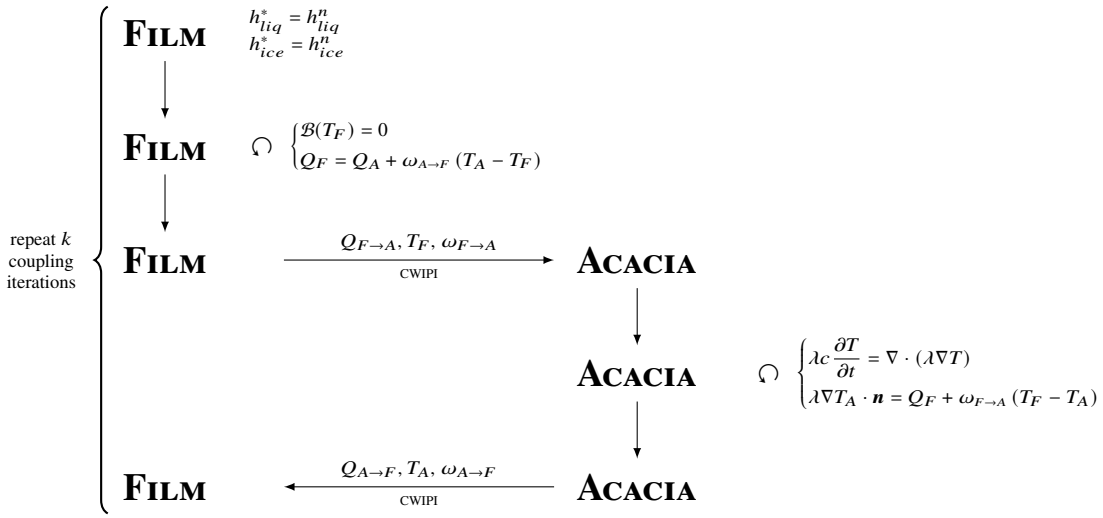

Fig. 12 Sketch of the coupling procedure occurring at each time step between the wall heat conduction solver ACACIA (designated by A) and the FILM accretion solver (designated by F).

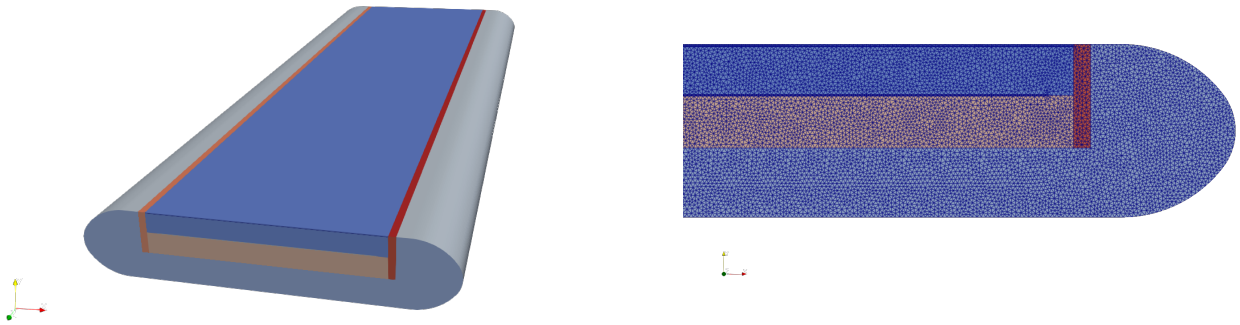

(a) Numerical model for the flat plate test-case.

(b) Side-view of the mesh for the flat plate test-case.

Fig. 13 Illustrations of the numerical model used for the "flat plate" simulation.

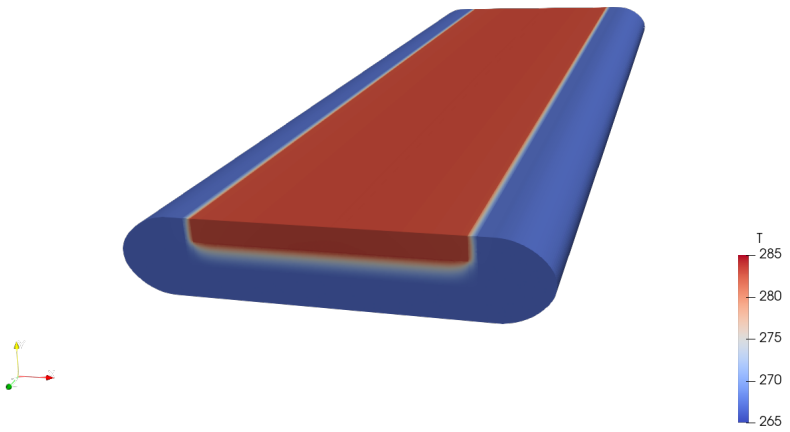

Fig. 14 Temperature in the solid for dry-air condition.

The experimental run that is simulated here corresponds to an upstream air temperature of 263 K, a pressure of 101 325 Pa and a Mach number of 0.12. Ice crystals are injected with a concentration of $IWC = 5 \times 10^{-3}$, a mean diameter of $MVD = 80\,\mu m$ and at thermal equilibrium with the air.

The simulation of the flow field and the crystals trajectories is not described here, but can be found in [5]. The first step before starting the coupling is to initialize the heat conduction solver (in the solid wall) with dry-air condition, as it is actually done in the experimentation. After a few minutes, the temperature in the solid reaches a steady temperature, with a surface temperature of approximately 10 degrees higher than the air temperature. The wall temperature field is depicted on figure 14 : the heaters lead to a higher temperature on the top while the opposite side, isolated by an insulated layer, reaches the air temperature. In order to focus on the coupling between the conduction and the accretion, this heat conduction initialization simulation has been calibrated to match as closely as possible the experimental results. This calibration has been performed by adjusting the heat transfer coefficient[¶].

Then the coupling can be started. As stated above, the choice of the coupling coefficients is the key ingredient to obtained a robust simulation. For the present case, a constant coefficient of $\omega = 10^4$ has been applied for the two solvers. This value has been found by trial and error and the simulation often quickly diverged with the different values tried except the neighborhood of this one. The number of coupling (sub-)iterations between each time steps is time-dependent : the evolution of this number during the simulation is depicted on figure 15. Note that some time steps require a lot of sub-iterations to converge while others don't. For some time steps, the required number of sub-iteration to meet the convergence criteria may be very high, hence a maximum of 50 sub-iterations has been imposed.

The settings for the accretion solver are the following : the sticking efficiency model and the porosity model can be found in Trontin & Villedieu [6] while the erosion model is the one from Charton *et al.* [8].

In the experiment, several temperature probes inside the solid record the temperature evolution over time. To compare the simulations results with the experimental data, the probe named PT1000-09 is selected. This probe is located at the center of the flat plate, just under the skin (less than 1 mm below the surface). The temperature evolution for the present coupled 3D simulation (designated as FILM - ACACIA), the 2D simulation (IGLOO2D) and the experimental data are depicted on figure 16. The coupled simulation only starts when ice crystals are injected ($t = 0$) while the experiment starts a few minutes earlier with dry-air conditions. Hence the dashed lines for FILM-ACACIA and IGLOO2D are only drawn for illustration purpose. Regarding the temperature temporal evolution, note that experimental temperature decreases from the dry-air temperature (283 K) to the melting point (273.15 K), in approximately 30 s or 40 s. In both the 2D and 3D simulations this temperature decrease is recovered, although the transitional regime does not accurately match the experimental one. The decrease is indeed more abrupt in the simulations than in the experiment. This difference may be explained by the limitation offered by the surface model used for the accretion solver. For instance only one temperature by (surface) cell is computed whereas in practice a temperature gradient

[¶]Note that this calibration only concerns the heat conduction solver initialization. Once the coupling is started, the transfer coefficient is provided by the accretion solver.

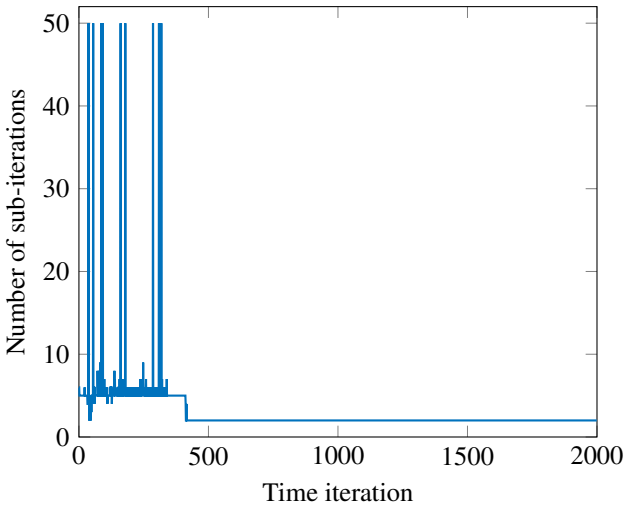

Fig. 15 Number of coupling iterations (= sub-iterations) for each time step.

could exist in the ice/liquid column at a given position on the surface. However the overall result is still satisfying in the sense that the developed models and the coupling algorithms enable to simulate the main physical phenomenon : a temperature decrease on the wall of a heated solid under ice crystal icing conditions. More over, since the 2D simulation results represent the reference results for the 3D solver, the latter figure validates the numerical implementation of the coupling algorithm. The slight differences between the two simulations lines can essentially be explained by the calibration performed for the dry-air initialization, which is different in the two simulations.

VI. Conclusion

MUSIC-haic European project gives to the authors the opportunity to update the ONERA 3D accretion tool, the Film solver, with ICI models. Especially to take into account erosion, porosity and thermal coupling with a wall.

The implementation of ICI models in 3D tools requires to develop specific methodologies since the approaches currently used for 2D simulations, such as the multi-step approach for example, remain too expensive for 3D simulations. In that way, in order to avoid re-meshing at each step, a new geometrical algorithm has been put forward in order to reproduce erosion effect on the ice shape. The first test-cases completed for 2D simulations demonstrate that the so-called Impact Angle Correction method delivers satisfactory results very efficiently. It demonstrates that for ICI modeling, the erosion effect on the ice shape prevails among other phenomena. Especially the modification of the gas flow-field and the particle trajectories. However the application of the IAC method to a 3D test-case shows that it can be influenced by a noisy mass impact flow field. Hence it implies to use a smoothing method, both for the collection efficiency and the ice shape and its gradients at each time step of the IAC method. Indeed, the IAC method seems more sensitive to numerical instabilities when it is being used on fine mesh as it is the case for the hemispherical 3D simulation. However first industrial applications presented in [19] show that promising results can be obtained in 3D without smoothing. The next step is thus to test the robustness of this method for many more cases, to analyze the effect of the mesh and to test this new method using other erosion models to evaluate the effect of the model(s).

Furthermore a strong coupling between the accretion and a heat conduction solver has been developed and validated on an experimental setup, also conducted in the MUSIC-haic project. This coupling is necessary as soon as the wall contains anti-icing or de-icing devices. The presented solution, using an open-source coupling library and a specific coupling algorithm, is suitable for 3D simulations. However, the convergence of such simulations is still hard to achieve and more studies are necessary to improve the current algorithms, especially the determination of coupling coefficients.

Acknowledgments

Funding from European Union's Horizon 2020 research and innovation program under agreement number 767560 is gratefully acknowledged.

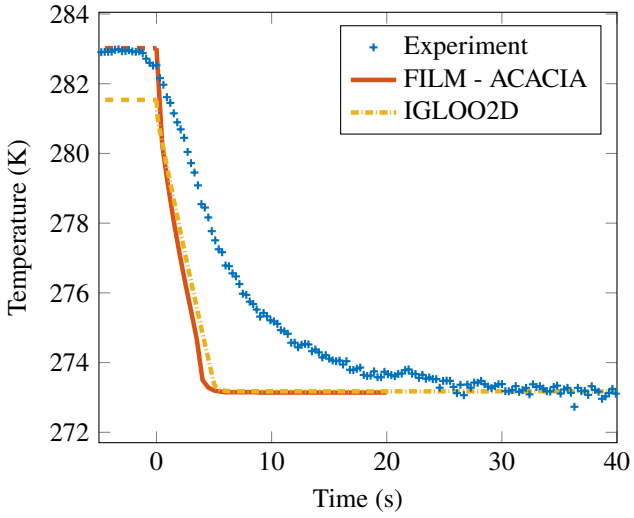

Fig. 16 Time evolution of the temperature inside the solid, less than 1 mm **below the interface. Crystal injection starts at** $t = 0$**.**

References

[1] Currie, T., and Fuleki, D., "Development and Application of an Impedance-Based Instrument for Measuring the Liquid Fraction and Thickness of Ice Crystal Accretions," Tech. rep., SAE Technical Paper, 2015.

[2] Refloch, A., Courbet, B., Murrone, A., Villedieu, P., Laurent, C., Gilbank, P., Troyes, J., Tessé, L., G., C., Dargaud, J. B., Quémerais, E., and Vuillot, F., "CEDRE Software," *AerospaceLab*, , No. 2, 2011, pp. 1–10. URL `https://hal.archives-ouvertes.fr/hal-01182463`.

[3] Gomez de Segura Solay, G., Radenac, E., Chauvin, R., and Laurent, C., "Simulations of ice accretion, runback and droplet re-emission in a multi-stage model of aeronautical engine," *8th AIAA Atmospheric and Space Environments Conference*, 2016, p. 4350.

[4] Hauk, T., Bonaccurso, E., Villedieu, P., and Trontin, P., "Theoretical and experimental investigation of the melting process of ice particles," *Journal of Thermophysics and Heat Transfer*, Vol. 30, No. 4, 2016, pp. 946–954.

[5] Villedieu, P., Trontin, P., and Chauvin, R., "Glaciated and mixed phase ice accretion modeling using ONERA 2D icing suite," *6th AIAA atmospheric and space environments conference*, 2014, p. 2199.

[6] Trontin, P., and Villedieu, P., "A comprehensive accretion model for glaciated icing conditions," *International Journal of Multiphase Flow*, Vol. 108, 2018, pp. 105–123.

[7] Norde, E., Senoner, J.-M., van der Weide, E. T. A., Trontin, P., Hoeijmakers, H. W. M., and Villedieu, P., "Eulerian and Lagrangian ice-crystal trajectory simulations in a generic turbofan compressor," *Journal of Propulsion and Power*, Vol. 35, No. 1, 2019, pp. 26–40.

[8] Charton, V., Trontin, P., Aouizerate, G., and Villedieu, P., "Semi-Empirical Modelling of Erosion Phenomena for Ice Crystal Icing Numerical Simulation," *SAE International Journal of Advances and Current Practices in Mobility*, Vol. 2, No. 2019-01-1967, 2019, pp. 106–114.

[9] Finnie, I., and McFadden, D., "On the velocity dependence of the erosion of ductile metals by solid particles at low angles of incidence," *Wear*, Vol. 48, No. 1, 1978, pp. 181–190.

[10] Bitter, J., "A study of erosion phenomena part I," *wear*, Vol. 6, No. 1, 1963, pp. 5–21.

[11] Bitter, J., "A study of erosion phenomena: Part II," *Wear*, Vol. 6, No. 3, 1963, pp. 169–190.

[12] Charton, V., Senoner, J.-M., Trontin, P., and Villedieu, P., "Semi-empirical Erosion Model with Particle Size and Liquid Water Content Effects for Ice Crystal Icing Simulations," *AIAA AVIATION 2020 FORUM*, 2020, p. 2827.

[13] Currie, T. C., Fuleki, D., and Mahallati, A., "Experimental studies of mixed-phase sticking efficiency for ice crystal accretion in jet engines," *6th AIAA Atmospheric and Space Environments Conference*, 2014, p. 3049.

[14] Currie, T. C., Fuleki, D., Knezevici, D. C., and MacLeod, J. D., "Altitude scaling of ice crystal accretion," *5th AIAA Atmospheric and Space Environments Conference*, 2013, p. 2677.

[15] Currie, T. C., and Fuleki, D., "Experimental results for ice crystal icing on hemispherical and double wedge geometries at varying mach numbers and wet bulb temperatures," *8th AIAA Atmospheric and Space Environments Conference*, 2016, p. 3740.

[16] Bennani, L., Trontin, P., Chauvin, R., and Villedieu, P., "A non-overlapping optimized Schwarz method for the heat equation with non linear boundary conditions and with applications to de-icing," *Computers & Mathematics with Applications*, Vol. 80, No. 6, 2020, pp. 1500–1522.

[17] Errera, M.-P., and Chemin, S., "Optimal solutions of numerical interface conditions in fluid–structure thermal analysis," *Journal of Computational Physics*, Vol. 245, 2013, pp. 431–455.

[18] Errera, M.-P., Lazareff, M., Garaud, J.-D., Soubrié, T., Douta, C., and Federici, T., "A coupling approach to modeling heat transfer during a full transient flight cycle," *International Journal of Heat and Mass Transfer*, Vol. 110, 2017, pp. 587–605. https://doi.org/https://doi.org/10.1016/j.ijheatmasstransfer.2017.03.048, URL https://www.sciencedirect.com/science/article/pii/S0017931016331222.

[19] Soubrié, T., Laurent, C., and Bouyges, M., "Ice accretion modelling in the ICE-MACR compressor rig," *AIAA*, 2022.